CHEMISTRY
AN ASIAN JOURNAL
Full Paper

Use of 6-Methylisoxanthopterin, a Fluorescent Guanine Analog, to Probe Fob1-Mediated Dynamics at the Stalling Fork Barrier DNA Sequences

Jessy Mariam,[a] G. Krishnamoorthy,*[b] and Ruchi Anand*[a]

Abstract: Fluorescent nucleic acid base mimics serve as excellent site-specific and real-time reporters of the local and global dynamics. In this work, using the fluorescent guanine mimic 6-methylisoxanthopterin (6-MI), we unravel the differential dynamics of replication fork barrier/terminator sequences (RFB1 and RFB3) mediated by fork blocking protein (Fob1). By strategic and site-specific incorporation of this probe, we show that 6-MI is able to capture the changes in global dynamics exhibited by Fob1 and aids in distinguishing between varied architectural forms like double-stranded DNA versus Holliday junctions (HJs). This is important as these barriers are hotspots for recombination. Fluorescence lifetime and anisotropy decay studies further revealed that Fob1 strongly dampens the dynamics in double-stranded RFB1, and the sequence inherently possesses lesser flexibility in comparison to RFB3. We show that 6-MI can probe the differential oligomeric status of Fob1 in response to various architectures, that is, double-stranded versus HJs. This work highlights the unique advantages of 6-MI as a probe when incorporated in nucleic acid frameworks.

Introduction

Clever designing and fabrication of fluorescent probes specific for nucleic acids is an emerging trend as nucleic acids are fluorescently silent. These probes serve as powerful tools with novel properties and a plethora of applications in nucleic acid sensing,[1] imaging[2] and in probing protein-nucleic acid interactions.[3] For instance, an innovative approach employing pyrene-locked nucleic acid-based oligonucleotides enabled detection of single-nucleotide polymorphisms in natural nucleic acid targets.[1a,4] There are several other popular end-labeling probes such as fluorescein, rhodamine, and cyanine dyes.[5] However, when site-specific dynamics within nucleic acid sequences are probed, there are only a handful of alternatives. This is because for internal DNA/RNA labeling it is more preferable to use close mimics that cause minimal structural perturbation while acting as effective readout tools. The most widely employed and one of the first to be discovered site-

specific fluorescent base analog 2-aminopurine (2-AP),[6] an adenosine analog is an excellent molecule as it exhibits optimal photophysical properties and is a very environment-sensitive probe.[7] However, 2-AP has a few drawbacks, it has a low quantum yield in a double-stranded setting[8] and its excitation wavelength overlaps with the intrinsic absorption edge of proteins. Therefore, several other probes, such as the red-shifted adenosine analog 6-MAP (4-amino-6-methyl-8-(2′-deoxy-β-D-ribofuranosyl)7(8H)-pteridone)[9] have been developed. Site-specific probes for other nucleobases with red-shifted profiles such as thienoguanosine,[10] a guanosine analog, pyrrolo probes which are cytidine analogs[11] have also been effectively employed to monitor nucleobase flipping,[10] secondary structure formation in RNA[12] and as a biosensor to monitor DNA glycosylase activity in human blood.[13] Probes with both enhanced quantum yield as well as optimal lifetime window such as 3-methylisoxanthopterin (3-MI) and 6-methylisoxanthopterin (6-MI) (Figure 1) are other fluorescent guanosine analogs in use.[14] For instance studies on 6-MI labeled human telomeric repeat DNA and unwinding protein (UP1) has established 6-MI to be a sensitive reporter of stacking and unstacking interactions upon protein binding.[15] 6-MI has also proved its utility in monitoring the dynamics of complex ribozyme architectures.[16] By strategic designing of a pentameric oligonucleotide con-

[a] Dr. J. Mariam, Prof. R. Anand
Department of Chemistry
Indian Institute of Technology Bombay
Powai, Mumbai 400076, Maharashtra (India)
E-mail: ruchi@chem.iitb.ac.in

[b] Prof. G. Krishnamoorthy
Department of Biotechnology
Anna University
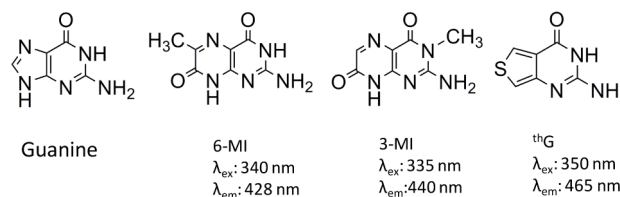Chennai 600025 (India)
E-mail: gk@tifr.res.in

Figure 1. Structure of guanine and its fluorescent mimics 6-methylisoxanthopterin (6-MI), 3-methylisoxanthopterin (3-MI), and thioguanine (thG).

taining 6-MI, this reporter demonstrated enhanced quantum yields permitting picomolar concentrations of DNA to be examined.[17]

Here, we investigate the ability of 6-MI to differentiate DNA architectures and oligomerization status of proteins. The model system that we have chosen is fork blocking protein (Fob1) which is known to stall replication forks within the ribosomal DNA (rDNA).[18] Replication fork barriers (RFBs) or terminator sequences (*ter*) are located within the rDNA (which comprises of 150–200 repeats)[19] and constitutes two regions *viz* RFB1 (*ter1*) and RFB3 (*ter2*) (Figure 2A). Replication forks pro-
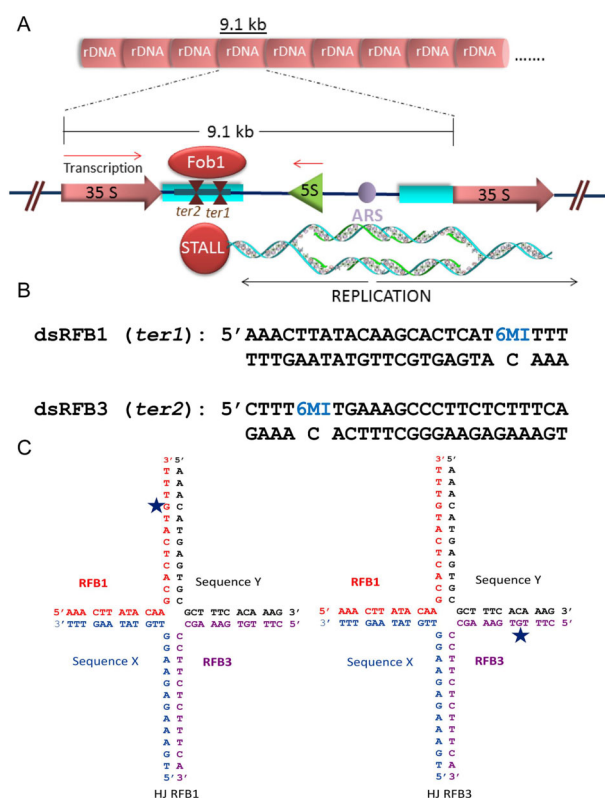

Figure 2. (A) Schematic representation of ribosomal DNA containing tandem repeats (each unit ≈ 9.1 kb) and terminator/barrier (*ter*) sequences (within a single unit of the ribosomal DNA repeat) binding to Fob1 and stalling the replication fork proceeding in the direction opposite to 35S transcription. Replication begins at autonomously replicating sequence (ARS) and proceeds bidirectionally (B) Double-stranded RFB constructs of 24 bp containing site-specifically incorporated 6-MI (C) Synthetic Holliday junctions, HJRFB1 and HJRFB3 containing 6-MI (denoted as a blue star) labeled RFB1 and RFB3 respectively.

gressing in a direction opposite to 35S transcription are stalled at these barriers by Fob1 (Figure 2A) in consort with other proteins, thereby preventing head-on collision with the transcription machinery.[20] This mechanism of preferential blocking via Fob1 prompts unidirectional transcription and thereby, confers genomic stability in yeast. The stalls in this process also create recombinogenic hotspots and result in excision of rDNA repeat,[21] influencing cellular aging.[22] Thus it appears that Fob1 likely has the potential of recognizing multiple DNA architectures such as double-stranded, polar fork blocks and Hol-

liday junctions (HJs). We have previously extensively studied the polar fork blocking ability of Fob1 by using 2-AP incorporated in synthetic forks.[23] Our studies revealed that Fob1 can differentiate between forks progressing from opposite directions and that it clamps few bases ahead of the fork, in the double-stranded region. However, considering the photophysical properties of 6-MI here to develop insights into differential interaction of Fob1 with HJs versus duplex DNA we have employed 6-MI as we believe it has a broader lifetime window. By designing synthetic HJs comprising of 6-MI labeled RFB1 and RFB3 we aim to address the question whether Fob1 has the ability for differential architectural recognition that is, if it can discriminate between double-stranded DNA versus Holliday junctions. Using the approach of fluorescence lifetime and anisotropy decay kinetics with 6-MI as the reporter we explore the binding and motional dynamics in double-stranded RFBs and model HJs.

Results and Discussion

Site-specific dynamics in duplex RFBs and Holliday junctions

To analyze the behavior of 6-MI as a probe, 24 bp sequences of RFB1 and RFB3 containing 6-MI were annealed with corresponding complementary sequences to form duplexes (dsRFB1 & dsRFB3) and HJs (HJRFB1 and HJRFB3) (Figure 2B,C). It was observed that steady-state anisotropy value of free dsRFB1 (0.13) was almost double as that of dsRFB3 (0.07) implying that RFB1 is inherently less flexible in comparison to RFB3. This significant difference further gets elaborated from time-resolved anisotropy. Figure 3A represents the anisotropy decay of
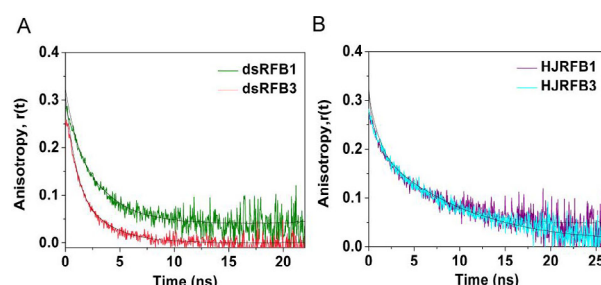

Figure 3. Anisotropy decay kinetics of site-specifically incorporated 6-MI DNA constructs A) duplex RFB1 versus duplex RFB3 (B) HJRFB1 versus HJRFB3.

dsRFB1 and dsRFB3. The decay curves fit best to a two-component model. The rotational correlation times and their amplitudes are summarized in Table 1. The shorter correlation time (Φ_1) represents segmental dynamics whereas the longer correlation time (Φ_2) represents global dynamics. The long correlation time for both the sequences was ≈ 3.2 ns (Table 1) and it is as expected for a DNA of 24 bp.[7b] A very interesting point to note in Figure 3A is that both the sequences have the same number of base pairs and identical near neighbors but yet they show a significant difference in their anisotropy decay. This implies that it is not the differences in the local motion

⬉⬉ These are not the final page numbers!

Table 1. Anisotropy decay parameters of dsRFB1, dsRFB3 HJRFB1 and HJRFB3 in the absence and presence of Fob1.

Construct	θ_1 [ns]	β_1	θ_2 [ns]	β_2	χ^2
dsRFB1	0.29 ± 0.01	0.45 ± 0.01	3.14 ± 0.05	0.55 ± 0.01	1.38
dsRFB1 + Fob1	1.68 ± 0.12	0.28 ± 0.02	92.72 ± 3.88	0.72 ± 0.02	1.49
dsRFB3	0.45 ± 0.06	0.67 ± 0.02	3.27 ± 0.27	0.33 ± 0.02	1.59
dsRFB3 + Fob1	0.68 ± 0.06	0.59 ± 0.01	12.12 ± 0.79	0.41 ± 0.01	1.55
HJRFB1	0.29 ± 0.10	0.46 ± 0.01	6.78 ± 0.30	0.54 ± 0.01	1.46
HJRFB1 + Fob1	0.60 ± 0.03	0.21 ± 0.01	49.18 ± 1.07	0.79 ± 0.01	1.33
HJRFB3	0.70 ± 0.02	0.37 ± 0.01	9.56 ± 0.05	0.63 ± 0.01	1.45
HJRFB3 + Fob1	2.07 ± 0.05	0.14 ± 0.01	52.90 ± 0.52	0.86 ± 0.01	1.57

rather it is the difference in the segmental or the long-range dynamics that is more prominent. A similar situation can be observed in the report by Moreno et al.,[17] wherein sequences comprising of 34 bp and flanked by adenine and thymine showed distinct anisotropy decays. Thus 6-MI is unusual in comparison to other probes as it is able to delineate the differences in the segmental dynamics of the two strands, which is generally not seen with commonly used probes like 2-AP. Another advantage of 6-MI, unlike 2-AP, is its long lifetime window that makes the measurement of very long correlation times possible. Thus both the short and long correlation times can be effectively exploited in analyzing and interpreting protein-DNA interactions.

HJs were constructed so as to contain 6-MI at the same position as that located in the double-stranded form, although the overall construct now takes up a different conformation. The longer correlation time, Φ_2 for HJs was approximately in the range of 7–9 ns (Table 1) which is expected as the molecular weight of HJ will be twice as that of the double-stranded form. Here again, we point out that the dynamics of the two HJ constructs are not identical. Thus even in the HJ constructs like the duplex RFBs, 6-MI was able to reveal the differences in sequence-dependent segmental dynamics.

Equilibrium binding studies of RFB-Fob1

Subsequent to studies on the dynamics of various DNA constructs we then studied their binding with Fob1. Binding studies were performed using steady-state fluorescence anisotropy and electrophoretic gel shift mobility assay. Binding curves of the four 6-MI constructs with Fob1 are shown in Figure 4A. Estimates of the equilibrium dissociation constants, K_d of all the four constructs were found to be similar in the range of 13–19 μm. Thus it can be concluded that the affinity of all the constructs to Fob1 is very similar. Electrophoretic mobility gel shift assays distinctly revealed the retardation of the RFBs in presence of Fob1 and corroborated the results obtained from steady-state anisotropy studies, indicating that the introduction of 6-MI into DNA did not alter its binding to Fob1 (Figure 4B–D). The gels also reveal a different pattern of binding for dsRFB1 (Figure 4B) wherein intermediate complexes are observed in between the unbound and saturated states, possibly indicating a co-operative mode of binding of Fob1 onto RFB1.
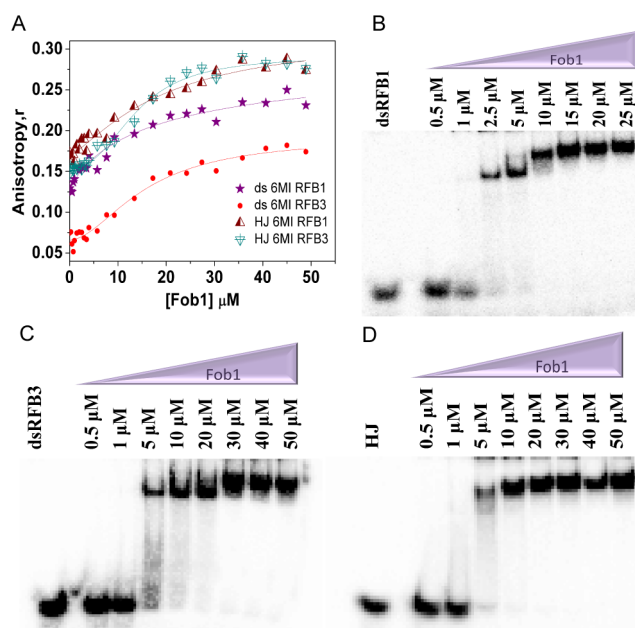

Figure 4. (A) Steady-state anisotropy binding curves of duplex RFB1, duplex RFB3, HJRFB1, and HJRFB3 (containing site-specifically incorporated 6-MI) with Fob1, $\lambda_{ex} = 340$ nm, $\lambda_{em} = 428$ nm (B–D) Electrophoretic mobility gel shift assay of 20 nm dsRFB1 (B) dsRFB3 (C) and HJ (D) with Fob1. For these assays, the constructs did not contain 6-MI and were labeled at the 5′ end with [γ-32P]-ATP. For dsRFB1, RFB1 was the radioactively labeled strand whereas in dsRFB3 and HJ construct, RFB3 was labeled.

Fluorescence intensity decay kinetics of duplex RFBs and HJs

Unlike 2-AP, which can base pair with cytosine (in wobble configuration) or thymine (in Watson–Crick geometry), 6-MI is a faithful mimic of guanine and has been shown to preferably hydrogen bond with cytosine.[24] The excited-state lifetime of free 6-MI is ≈6.3 ns[14a] which is very similar to that of 2-AP, ≈10 ns.[7a] Both free 6-MI and 2-AP exhibit a very high quantum yield of 0.70[14a] and 0.68[6] respectively. However, when incorporated into single-stranded (ss) DNA the quantum yield of 2-AP dramatically falls by more than 10-fold,[23] whereas 6-MI exhibits less than four-fold reduction (Table T1).[17] In our ss6-MI RFB1 sequence we obtained a quantum yield of 0.23 (Table T1), which is slightly higher than some 6-MI and 3-MI reported sequences, flanked by thymine bases.[25] Upon conversion to the double-stranded form, the quantum yield of our 6-MI sequences almost remained the same (Table T1 and 2). Contrastingly for 2-AP, it is observed that fluorescence is further quenched in a double-stranded (ds) setting. Our earlier studies clearly show that every time 2-AP is incorporated in an RFB1 variant the quantum yield reduces by at least 10 fold.[23] Whereas, we show here that 6-MI has almost no change in quantum yield between ss and ds settings (Table T1). This makes 6-MI a preferred probe to measure site-specific dynamics. In case of sequences studied by Knutson and group[25] and Moreno et al.,[17] wherein 6-MI was flanked by adenine or thymine bases, an enhancement in quantum yield was observed. In fact, flanking by thymines demonstrated a novel effect of

These are not the final page numbers! ↗↗

doubling of quantum yield on duplex formation.[25] Enhancement in quantum yield could be attributed to the presence of neighboring insulating nucleobases.[26] Thus in this scenario unlike 2-AP containing oligonucleotides wherein quenching occurs upon duplex formation, in 6-MI RFB1 low quenching effects are observed. Thus 6-MI can be considered to be a brighter fluorophore when compared to 2-AP.

It was observed that the fluorescence intensity decay of 6-MI labeled constructs fits to a sum of three exponentials (Table 2). The longest lifetime is suggested to correspond to an

Table 2. Fluorescence intensity decay parameters of dsRFB1, dsRFB3 HJRFB1, and HJRFB3 in the absence and presence of Fob1.

Construct	τ_1 [ns] $[\alpha_1]$	τ_2 [ns] $[\alpha_2]$	τ_3 [ns] $[\alpha_3]$	τ_m [ns]	$\chi2$
ssRFB1	0.25 (0.39)	1.85 (0.41)	5.63 (0.20)	1.97	1.03
dsRFB1	0.17 (0.61)	1.87 (0.23)	5.84 (0.16)	1.40	1.10
dsRFB1+Fob1	0.32 (0.52)	2.09 (0.29)	5.96 (0.19)	1.85	1.20
dsRFB3	0.38 (0.33)	3.75 (0.21)	6.80 (0.46)	4.04	1.10
dsRFB3+Fob1	0.42 (0.25)	2.56 (0.17)	6.21 (0.58)	4.12	1.10
HJRFB1	0.18 (0.59)	2.14 (0.12)	5.65 (0.29)	1.98	1.61
HJRFB1+Fob1	0.32 (0.45)	3.71 (0.17)	5.76 (0.38)	2.95	1.28
HJRFB3	0.40 (0.30)	4.99 (0.15)	7.33 (0.55)	4.87	1.10
HJRFB3+Fob1	0.40 (0.36)	4.87 (0.14)	7.17 (0.50)	4.41	1.57

extrahelical conformation of 6-MI as this value is close to that of free 6-MI.[14a] The shortest lifetime likely arises from 6-MI stacking with adjacent bases (a suggestion similar to the observations in 2-AP[7]). The second lifetime value represents an intermediate conformation between the two states. However, it should be mentioned that the assignment of conformational states based on fluorescence lifetimes is largely speculative in the absence of direct structural studies. The shortest lifetime in 6-MI labeled sequences is no shorter than 170 ps (Table 2) which makes it again a more useful probe than 2-AP. On addition of Fob1 in the case of dsRFB1, although the data still fits to a sum of three exponential the mean lifetime increased by 450 ps. Enhancement in mean lifetime could be attributed to restricted local dynamic motion, reduced solvent accessibility and base stacking interactions upon binding to Fob1. Restricted local dynamic motion is evident from the short correlation times of RFB1-Fob1 in comparison to RFB3-Fob1 (Table 1). Contrastingly, for dsRFB3 a decrease in mean lifetime was observed on Fob1 binding. This reduction in lifetime could be attributed to dynamic quenching upon binding to Fob1. A similar scenario is observed in another system studied by Moreno et al., where binding of integration host factor protein to its cognate 6-MI labeled DNA results in decreased lifetime.[17] It was further observed that the mean lifetimes of the RFB1-RFB3 composite

HJs were similar to that of the double-stranded form (Figure S1, Table 2). Upon binding to Fob1 a similar increase in lifetime by 970 ps and a decrease in lifetime by 460 ps were observed for HJRFB1 and HJRFB3 respectively (Table 2). Although no dramatic changes in lifetime were observed on protein binding, if we make a relative comparison in mean lifetime across different architectures, we observe that RFB1 containing constructs show a higher change on binding to Fob1 and are hence more sensitive to perturbation by protein. Hence, it appears this probe although not as sensitive as 2-AP[23] in this window can still guide towards yielding qualitative information regarding the binding.

Fob1 mediated altered dynamics in duplex RFBs and HJs

Although 6-MI doesn't appear to be as sensitive in the fluorescence lifetime regime it appears to be an excellent probe for fluorescence anisotropy decay kinetics experiments. As discussed earlier 6-MI was incorporated in diverse architectures such as double stranded and HJs where it exhibits sensitivity in anisotropy decay kinetics and was able to clearly distinguish between diverse secondary structures. Therefore, to study if these differences are further enhanced in the presence of protein we carried out these studies in the presence of Fob1. Here again, we observe that 6-MI is very sensitive towards the addition of protein and marked changes are observed in different samples. Analyzing the anisotropy decay kinetics of dsRFB1 and dsRFB3 in presence of Fob1 revealed that upon binding of Fob1 to dsRFB1, Φ_1 increased to ≈ 1.7 ns implying that the local motion of 6-MI is constrained with respect to the free dsRFB1 sequence (Figure 5A). Contrastingly dsRFB3 in presence of Fob1 faced a lesser restriction locally as can be observed by a nominal increase in Φ_1 (Figure 5B, Table 1). Thus the addition of Fob1 places 6-MI in a more restricted environment in RFB1 as compared to RFB3. This difference is more ap-
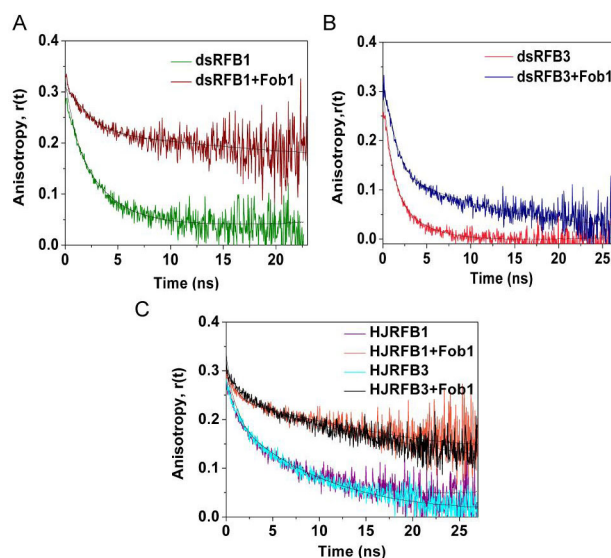

Figure 5. Time-resolved anisotropy decay curve of 6-MI labeled RFBs A) dsRFB1 with and without Fob1 (B) dsRFB3 with and without Fob1 (C) Site-specific 6-MI labeled HJRFB1 and HJRFB3 with and without Fob1.

↖↖ **These are not the final page numbers!**

parent when Φ_2 values are compared across the two double-stranded sequences. The longer correlation time, Φ_2, of dsRFB1 in presence of Fob1 exhibits a dramatic increase to ≈ 90 ns, thereby strongly dampening the dynamics of dsRFB1. This large dampening in dynamics was not observed in dsRFB3 as Φ_2 increased to only around 12 ns. This indicates that perhaps in presence of RFB1, Fob1 forms larger protein aggregates or dsRFB3-Fob1 does not represent the global dynamics but could represent segmental dynamics. To further confirm the oligomeric state of the protein, we measured anisotropy decay kinetics of fluorescamine-Fob conjugates (described in supporting information). The free form of fluorescamine dye is not fluorescent but when it reacts with ϵ- amino group of lysines in proteins to form conjugates it becomes fluorescent exhibiting a lifetime of 3–9 ns.[27] Thus with a large lifetime window fluorescamine serves as a suitable ruler to deduce associated forms of the protein in fluorescence anisotropy decay settings as long correlation times can be estimated. Fitting the fluorescence anisotropy decay of fluorecscamine-Fob conjugate, a global correlation time of 90 ns was obtained (Figure S2). A protein with a molecular weight of 25 kDa has been generally reported to have a rotational correlation time of near 10 ns.[28] Therefore, we can conclude that Fob1 with a molecular mass of approximately 52 kDa is a tetramer. The rotational correlation time of 90 ns, was also observed for the ds 6-MI RFB1 sequence in presence of Fob1 indicating that RFB1 also binds Fob1 as a tetramer. Similar estimation of the oligomeric form of protein from the long correlation time has been reported for probes such as 3-MI, for HIV-1 integrase protein bound to its cognate DNA.[29] Thus it appears that the MI class of compounds can be used to deduce multimeric states of protein with high fidelity.

As mentioned earlier long correlation time Φ_2 of 12 ns was observed for dsRFB3. Our analysis reveals that this could arise if RFB3 is unable to form a stable oligomeric complex. Figure 3 A already indicates that RFB1 presents a more rigid scaffold as compared to RFB3. Hence, it is not surprising if RFB3 is unable to provide a suitable platform for stable oligomerization. Here, fluorescence anisotropy studies clearly revealed distinct differential restriction of dsRFB1 and dsRFB3 by Fob1, with the dsRFB1 facing a dominant restriction. This reflects the power of the long lifetime of 6-MI in revealing the nature of oligomerization of Fob1 when bound to the DNA constructs.

Further, to understand how RFB1 and RFB3 sequences behave in HJ architecture in presence of Fob1, fluorescence anisotropy decay kinetics with the identical complexes where the 6-MI is placed in different positions were performed. Results (Table 1) reveal that Φ_1 for HJRFB3+ Fob1 is almost three-fold that of HJRFB1+ Fob1. This trend is reverse of what has been observed in double-stranded architectures where RFB1 showed enhanced restriction. This switch could be because RFB3 is known to be a sequence that promotes recombination in presence of Fob1 and hence may restrict RFB3 dynamics more efficiently in HJ architecture. Further Φ_2 values of approximately 50 and 53 ns were observed, respectively for HJRFB1 and HJRFB3 sequences (Figure 5 C, Table 1). This again implies that in HJ architecture the oligomerization state of

Fob1 may differ from that in double-stranded sequences. Fob1 likely only tetramerizes when it is presented with the correct double-stranded barrier sequence, RFB1. In HJ it is possible that a dimeric form of Fob1 is the preferred form. Overall, these studies highlight the extreme sensitivity of 6-MI in the fluorescence decay kinetics regime.

Conclusions

6-MI proved to be a highly useful probe in decoding sequence-dependent segmental dynamics in DNA. Through anisotropy decay kinetics, this probe enabled recognition of varied DNA architectures such as double-stranded DNA and Holliday junctions. 6-MI as a reporter could thus bring out sequence- as well as structure-based readout of dynamics. Protein binding further enhanced this discrimination and revealed a distinct differential restriction of the two barrier sequences. Most importantly, 6-MI could provide insights into how the protein could adopt varied oligomeric forms depending on the DNA architecture. These powerful features of 6-MI can be exploited in understanding dynamics in nucleoprotein complexes which may be unfeasible/difficult to extract by other probes or techniques.

Experimental Section

Oligonucleotides

Modified oligonucleotides (PAGE purified) containing 6-MI were ordered from Fidelity Systems, Inc, Gaithersburg. Sequences of oligonucleotides used in this study are RFB1: 5′-AAACTTATACAAGCACTCAT6-MITTT-3′, RFB3: 5′-CTTT6-MITGAAAGCCCTTCTCTTTCA-3′, X: 5′-AAACATGAGTGCGCTTTCACAAAG-3′, Y: 5′-TGAAAGAGAAGGTTGTA-TAAGTTT-3′. Crude unlabelled oligonucleotides were purchased from Integrated DNA technologies and purified using 15% denaturing polyacrylamide gel. Oligonucleotides were visualized by UV shadowing and eluted from the gel. Duplex and cruciform DNA formation (sequence depicted in Figure 2 B, C) was achieved by mixing concentrations of unlabelled oligonucleotides 1.2 times the concentration of labeled oligonucleotides in 1X annealing buffer (10X: 50 mM Tris, 150 mM NaCl, pH 8) and heating at 95° C for 5 min followed by slow cooling to room temperature. For annealing of cruciform DNA, the buffer additionally contained 1.5 mM MgCl$_2$. Concentrations of single-stranded oligonucleotides were estimated by measuring the absorbance at 260 nm and extinction coefficients were taken as stated by the manufacturer. Four annealed constructs were used in this study. Two of them are duplexes of RFB1 and RFB3 and are designated in the text as dsRFB1 and dsRFB3. The other two constructs are HJs, designated in the text as HJRFB1 (contained the 6-MI labeled RFB1 and the other three strands are unlabelled) and HJRFB3 (6-MI labeled RFB3 and the remaining were unlabelled sequences).

Cloning and protein purification

Native Fob1 protein (1–450 amino acid residues) with N-terminal His tag was overexpressed and purified according to the established lab protocol, as described in Biswas et al.,[23] Briefly, an overnight culture of Rosetta cells transformed with Fob1 plasmid was inoculated into 1.2 liters of Luria Bertani broth containing kanamycin (35 μg mL^{-1}) and chloramphenicol (30 μg mL^{-1}) and incubated

at 37 °C, 220 rpm. The cells were induced in mid-log phase ($O.D_{600nm} \approx 0.6$) with 0.8 mM IPTG (Isopropyl β-D-1-thiogalactopyranoside) and grown at 25 °C. The cells were harvested after 6 hrs by centrifugation (4500 rpm, 20 min) and stored at −80 °C. Cell pellets were thawed quickly and suspended in buffer A (50 mM HEPES, 500 mM NaCl, 5 mM imidazole). Cells were then lysed by sonication and the lysate was centrifuged at 14 000 rpm, 4 °C for 1 h. The supernatant was mixed with Ni-NTA beads which were equilibrated with buffer A and placed on a rocker for 1 h. Thereafter the beads were centrifuged at 1200 rpm and loaded onto a column wherein the washing step was carried out with buffer B (50 mM HEPES, 500 mM NaCl, 15 mM imidazole). Gradient elution of the protein was performed with buffer containing 50 mM HEPES, 500 mM NaCl, 150 mM imidazole, followed by 200 mM imidazole. Fractions containing Fob1 were pooled and desalted in desalting columns equilibrated with desalting buffer (35 mM HEPES, 250 mM NaCl, 3% glycerol, 1 mM DTT). Fob1 was finally eluted with desalting buffer. The pooled fractions were concentrated in Corning concentrators. pH of all buffers was maintained at 7.5. Protein concentration was determined by measuring absorbance at 280 nm and using molar extinction coefficient value of $53\,290\ L\,mol^{-1}\,cm^{-1}$.

Steady-state fluorescence anisotropy

Steady-state anisotropy measurements of the four 6-MI constructs were performed on Cary Varian spectrofluorimeter with a manual polarizer. The samples contained 1 μM DNA in 25 mM HEPES and 50 mM NaCl buffer. Fob1 was titrated and each titration was under an incubation period of 4 mins. The excitation wavelength was set to 340 nm and emission was monitored at 428 nm with slit widths of 10 nm. The binding curves were fit to the following equation [Eq. (1)] to determine the equilibrium dissociation constant, K_d.[30]

$$r = r_0 + (r_1 - r_0)\left[\frac{1}{1 + (K_d/[Fob1])^n}\right] \tag{1}$$

where r_0 and r_1 represent the anisotropy of the free and bound DNA.

Anisotropy was calculated using the following equation [Eq. (2)]

$$r = \frac{I_{11} - GI_\perp}{I_{11} - 2GI_\perp} \tag{2}$$

Where $I_\|$ and $I_\perp$ are polarized parallel and perpendicular fluorescence intensities with respect to the vertically polarized excitation. G factor was estimated from the parallel and perpendicular fluorescence intensities with respect to the horizontally polarized excitation using the same sample.

Electrophoretic gel shift mobility assay

To confirm the binding of Fob1 to dsRFBs and HJs, electrophoretic mobility gel shift assays were performed. 20 picomoles of single-stranded RFB1 and RFB3 were radiolabelled at the 5′end using [γ-^{32}P]-ATP (3000 Ci/mmole) and T4 polynucleotide kinase (details in supporting information). In dsRFB3 and HJ construct, the single-stranded RFB3 sequence (5′-CTTTGTGAAAGCCCTTCTCTTTCA-3′) was the labeled strand whereas in dsRFB1 the sequence 5′- AAACT-TATACAAGCACTCATGTTT-3′was radiolabeled. The labeled RFBs were then annealed with their complementary strand at 90 °C for 5 min and allowed to gradually cool down. Reaction mixtures (10 μL) were prepared by incubating 1X binding buffer (10X: 10 mM HEPES, pH 7.8, 50 mM KCl, 1.8 mM DTT, 2 μg mL^{-1} BSA and

7.4% glycerol), protein in the concentration range of 50 nM to 50 μM and 20 nM radiolabeled DNA for 15 mins. The final volume was made up using desalting buffer. The samples were electrophoresed through native 6% polyacrylamide gel in Tris-borate EDTA buffer, pH 8 at 4 °C. For samples containing HJs, composite polyacrylamide gels of 6% (lower three-fourth of gel) and 5% (upper one-fourth) were used to facilitate the entry of the complex into the gel. Post electrophoresis run at 100 V, the gel was fixed in gel fixing solution (20 mL methanol, 10 mL acetic acid, 70 mL water) for 10 min, dried, covered in a saran wrap and exposed overnight at 4 °C in a phosphoimager cassette. At the end of exposure, gel images were captured by scanning the screen on Storm25 Phosphoimager.

Time-resolved fluorescence intensity

Fluorescence decays have been recorded on time-correlated single photon counting (TCSPC) system (IBH, UK) with excitation from a pulsed light emitting diode (ex: 340 nm). The full width at half-maximum of the instrument function was found to be 790 ps with a resolution of 14 ps per channel. The emission (428 nm) polarizer was kept at the magic angle (54.7°) with respect to the polarization of the excitation light. The lifetime decay curves were analyzed using a non-linear least-squares iterative deconvolution method based on the Levenberg-Marquardt algorithm (homemade software—N.Periasamy) and expressed as a sum of exponentials as follows [Eq. (3)]

$$I(t) = \sum_{i=1} \alpha_i e^{(-t/\tau_i)} \tag{3}$$

where τ_i is the individual lifetime with associated amplitude α_i and $\Sigma\alpha_i = 1$. The goodness of fits was determined from the reduced χ^2 and randomness of residuals. The mean lifetime τ_m is determined from $\Sigma\alpha_i\,\tau_i$

Time-resolved fluorescence anisotropy

For time-resolved anisotropy, decays were recorded using vertical/vertical ($I_\|$) polarization and vertical/horizontal ($I_\perp$) polarization upto difference of 5000 counts in the peak channel. The decay was analyzed using the following equations [Eqs. (4)–(7)]:

$$I_{11}(t) = I(t)[1 + 2r(t)]/3 \tag{4}$$

$$I_\perp = I(t)[1 - r(t)]/3 \tag{5}$$

$$r(t) = \frac{I_{11}(t) - G(\lambda)I_\perp(t)}{I_{11}(t) - 2G(\lambda)I_\perp(t)} \tag{6}$$

$$r(t) = r_0[\beta_1 e^{-(t/\phi_1)} + \beta_2 e^{-(t/\phi_2)}] \tag{7}$$

where $I_\|$ and $I_\perp$ are the intensities recorded at emission polarizations parallel and perpendicular, respectively to that of the incident polarized light, $G(\lambda)$ is the geometry factor at the emission wavelength λ, estimated using a very dilute solution of quinine sulfate. β_1 and β_2 are the amplitudes of the rotational correlation times Φ_1 and Φ_2 respectively such that $\Sigma\beta_i = 1$, r_0 is the initial anisotropy value determined independently for a sample in 50% glycerol and the value being extrapolated from the anisotropy decay curve to zero time. For time-resolved measurements, the samples contained 3 μM of DNA and 15 μM Fob1 in 25 mM HEPES and 50 mM NaCl buffer. Several decay profiles were collected for the same as well as independent sample sets. The decay values were averaged from

↖↖ These are not the final page numbers!

at least three data sets and represented with their standard deviations.

Conflict of interest

The authors declare no conflict of interest.

[1] a) T. S. Kumar, A. Myznikova, E. Samokhina, I. K. Astakhova, *Artif. DNA PNA XNA* **2013**, *4*, 58–68; b) M. H. Hu, X. Chen, S. B. Chen, T. M. Ou, M. Yao, L. Q. Gu, Z. S. Huang, J. H. Tan, *Sci. Rep.* **2015**, *5*, 17202.

[2] M. E. Østergaard, P. Cheguru, M. R. Papasani, R. A. Hill, P. J. Hrdlicka, *J. Am. Chem. Soc.* **2010**, *132*, 14221–14228.

[3] a) S. F. Singleton, A. I. Roca, A. M. Lee, J. Xiao, *Tetrahedron* **2007**, *63*, 3553–3566; b) D. Hamdane, A. Guelorget, V. Guérineau, B. Golinelli-Pimpaneau, *Nucleic Acids Res.* **2014**, *42*, 11697–11706.

[4] I. K. Astakhova, E. Samokhina, B. R. Babu, J. Wengel, *ChemBioChem* **2012**, *13*, 1509–1519.

[5] a) K. Wojtuszewski, I. Mukerji, *Biochemistry* **2003**, *42*, 3096–3104; b) J. M. Fogg, M. Kvaratskhelia, M. F. White, D. M. J. Lilley, *J. Mol. Biol.* **2001**, *313*, 751–764; c) J. R. Unruh, G. Gokulrangan, G. H. Lushington, C. K. Johnson, G. S. Wilson, *Biophys. J.* **2005**, *88*, 3455–3465; d) T. A. Windgassen, M. Leroux, K. A. Satyshur, S. J. Sandler, J. L. Keck, *Proc. Natl. Acad. Sci. USA* **2018**, *115*, E9075–E9084.

[6] D. C. Ward, E. Reich, L. Stryer, *J. Biol. Chem.* **1969**, *244*, 1228–1237.

[7] a) S. V. Avilov, E. Piemont, K. Shvadchak, H. de Rocquigny, Y. Mély, *Nucleic Acids Res.* **2008**, *36*, 885–896; b) N. Nag, B. J. Rao, G. Krishnamoorthy, *J. Mol. Biol.* **2007**, *374*, 39–53.

[8] T. Goel, T. Mukherjee, B. J. Rao, G. Krishnamoorthy, *J. Phys. Chem. B* **2010**, *114*, 8986–8993.

[9] a) M. E. Hawkins, W. Pfleiderer, O. Jungmann, F. M. Balis, *Anal. Biochem.* **2001**, *298*, 231–240; b) K. E. Augustyn, K. Wojtuszewski, M. E. Hawkins, J. R. Knutson, I. Mukerji, *Biochemistry* **2006**, *45*, 5039–5047.

[10] V. Kilin, K. Gavvala, N. P. F. Barthes, B. Y. Michel, D. Shin, C. Boudier, O. Mauffret, V. Yashchuk, M. Mousli, M. Ruff, F. Granger, S. Eiler, C. Bronner, Y. Tor, A. Burger, Y. Mély, *J. Am. Chem. Soc.* **2017**, *139*, 2520–2528.

[11] D. A. Berry, K. Y. Jung, D. S. Wise, A. D. Sercel, W. H. Pearson, H. Mackie, J. B. Randolph, R. L. Somers, *Tetrahedron Lett.* **2004**, *45*, 2457–2461.

[12] R. A. Tinsley, N. G. Walter, *RNA* **2006**, *12*, 522–529.

[13] C. Y. Lee, K. S. Park, H. G. Park, *Biosens. Bioelectron.* **2017**, *98*, 210–214.

[14] a) M. E. Hawkins, W. Pfleiderer, F. M. Balis, D. Porter, J. R. Knutson, *Anal. Biochem.* **1997**, *244*, 86–95; b) D. Jose, S. E. Weitzel, W. A. Baase, M. M. Michael, P. H. von Hippel, *Nucleic Acids Res.* **2015**, *43*, 9291–9305; c) M. E. Hawkins, F. M. Balis, *Nucleic Acids Res.* **2004**, *32*, e62.

[15] J. C. Myers, S. A. Moore, Y. Shamoo, *J. Biol. Chem.* **2003**, *278*, 42300–42306.

[16] X. Shi, E. T. Mollova, G. Pljevaljčić, D. P. Millar, D. Herschlag, *J. Am. Chem. Soc.* **2009**, *131*, 9571–9578.

[17] A. Moreno, J. Knee, I. Mukerji, *Biochemistry* **2012**, *51*, 6847–6859.

[18] T. Kobayashi, *Mol. Cell Biol.* **2003**, *23*, 9178–9188.

[19] T. D. Petes, *Proc. Natl. Acad. Sci. USA* **1979**, *76*, 410–414.

[20] a) B. J. Brewer, D. Lockshon, W. L. Fangman, *Cell* **1992**, *71*, 267–276; b) T. Kobayashi, M. Hidaka, M. Nishizawa, T. Horiuchi, *Mol. Gen. Genet.* **1992**, *233*, 355–362.

[21] a) K. Johzuka, T. Horiuchi, *Genes Cells* **2002**, *7*, 99–113; b) T. Kobayashi, D. J. Heck, M. Nomura, T. Horiuchi, *Genes Dev.* **1998**, *12*, 3821–3830.

[22] a) P. A. Defossez, R. Prusty, M. Kaeberlein, S. J. Lin, P. Ferrigno, P. A. Silver, R. L. Keil, L. Guarente, *Mol. Cell* **1999**, *3*, 447–455; b) D. A. Sinclair, L. Guarente, *Cell* **1997**, *91*, 1033–1042.

[23] A. Biswas, J. Mariam, M. Kombrabail, S. Narayan, G. Krishnamoorthy, R. Anand, *ACS Omega* **2017**, *2*, 7389–7399.

[24] K. Datta, N. P. Johnson, G. Villani, A. H. Marcus, P. H. von Hippel, *Nucleic Acids Res.* **2012**, *40*, 1191–1202.

[25] K. Wojtuszewski Poulin, A. V. Smirnov, M. E. Hawkins, F. M. Balis, J. R. Knutson, *Biochemistry* **2009**, *48*, 8861–8868.

[26] J. N. Wilson, Y. Cho, S. Tan, A. Cuppoletti, E. T. Kool, *ChemBioChem* **2008**, *9*, 279–285.

[27] a) R. F. Chen, *Anal. Lett.* **1974**, *7*, 65–77; b) J. F. Eccleston, E. Gratton, D. M. Jameson, *Biochemistry* **1987**, *26*, 3902–3907.

[28] J. R. Lakowicz, *Principles of fluorescence spectroscopy, 2nd ed.*, New York, Kluwer Academic/Plenum, **2006**, pp. 353.

[29] E. Deprez, P. Tauc, H. Leh, J. F. Mouscadet, C. Auclair, M. E. Hawkins, J. C. Brochon, *Proc. Natl. Acad. Sci. USA* **2001**, *98*, 10090–10095.

[30] a) A. V. Hill, *J. Physiol.* **1910**, *40*, 4–7; b) J. M. Pagano, C. C. Clingman, S. P. Ryder, *RNA* **2011**, *17*, 14–20.

FULL PAPER

*Jessy Mariam, G. Krishnamoorthy,**
*Ruchi Anand**

■■ – ■■

Use of 6-Methylisoxanthopterin, a Fluorescent Guanine Analog, to Probe Fob1-Mediated Dynamics at the Stalling Fork Barrier DNA Sequences
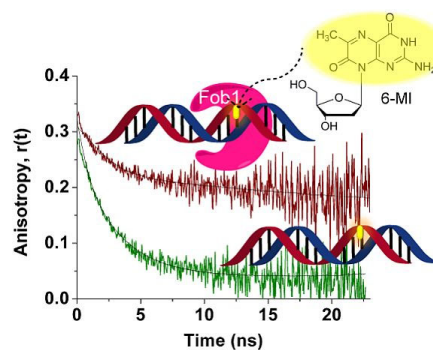
6-Methylisoxanthopterin (6-MI), a fluorescent guanine mimic was employed to capture the dynamics in duplex replication fork barrier sequences and Holliday junctions. In the presence of fork-blocking protein, the dynamics of duplex barriers were dampened dramatically. This paper highlights the powerful features of 6-MI in comparison to the fluorescent adenine analog, 2-amino-purine.

↖↖ These are not the final page numbers!